

# Prediction of the influence of solar radiation on adaptive thermal comfort using CFD simulation

Juti Hu<sup>\*1</sup>, Ge Song<sup>1</sup>, Guoqiang Zhang<sup>1</sup>

*1 Hunan Engineering Research Center for Intelligent Sunshading and High Performance Door and Window, National Joint Research Center for Building Safety and Environment, Department of Civil Engineering, Hunan University*

*Lushan South Road 2*

*Changsha, China*

*\*Corresponding author: 15857168423.163.com*

## ABSTRACT

Adaptive thermal comfort model has been widely used to evaluate the thermal comfort level of natural ventilation buildings. However, current adaptive standards offer a simple linear relationship between the outdoor temperature and the indoor comfort temperature, ignoring the influence of solar radiation. In this paper, CFD model is used to evaluate the thermal comfort of a residential building under natural ventilation conditions. Keeping the input parameters of outdoor temperature and wind speed and changing the input parameters of solar radiation to simulate the distribution of indoor air temperature and velocity. The results are compared with adaptive thermal comfort temperatures to predict global and local indoor thermal comfort. The results show that the presence or absence of direct sunlight has a great influence on indoor thermal comfort at the same outdoor temperature; in the absence of direct sunlight, the thermal sensation is relatively more uniform, and solar radiation has a significant effect on local thermal sensation.

## KEYWORDS

thermal comfort

CFD model

solar radiation

## 1 INTRODUCTION

The adaptive thermal comfort model proposes that people can adapt to environmental changes in a certain range by adding or subtracting clothes and opening and closing windows, which makes it possible to save unnecessary energy consumption of refrigeration and heating, and at the same time ensures the thermal comfort requirements by limiting the scope of application. Richard de Dear (Richard de Dear, 2001) found a significant correlation between indoor comfort and outdoor air temperature through statistical analysis of large databases of comfort research results from all over the world. Thereafter, C. Bouden (G. Carrilho, 2005) conducted a field survey of thermal comfort in five towns in two climate zones in Tunisia, and found that thermal sensation was related to the average outdoor temperature and the average outdoor operating temperature. The significance of outdoor parameters was further clarified. From that, the model describing the relationship between outdoor temperature and comfort temperature is widely used in the thermal comfort standard of natural ventilation in various countries. Therefore, it is possible to predict human thermal sensation under natural ventilation by using indoor and outdoor temperature parameters.

The CFD numerical simulation method fully considers the influence of actual factors on the ventilation process, and the simulation cost is low. It can obtain real-time three-dimensional data of the airflow characteristics in the ventilated room. It has become an indispensable tool for the study of natural ventilation. J.I. Peren et al. (J.I. Peren, 2015) used CFD to simulate the effect of different positions of asymmetric openings on cross ventilation in buildings. H. Montazeri and F. Montazeri (H. Montazeri, 2018) simulates the effect of the outlet opening of the roof windshield on the cross ventilation of buildings by CFD. The results show that the use of the outlet hole near the wind trap will not increase the induced air flow, but will lead to a significant decrease in indoor air quality. Because CFD software includes not only flow model, but also energy model and mass transfer model, CFD tools can also solve more complex problems of flow and heat transfer coupling. Xiufeng Yang and Ke Zhong (Xiufeng Yang, 2015) used CFD to simulate the changes of transient temperature and wind speed fields of hot-pressure ventilation, and verified the number of transient hot-pressure ventilation. The results show that the transient development of airflow and temperature distribution are different under different indoor and outdoor temperature differences. Using CFD to simulate the temperature and velocity fields to obtain the environmental parameters needed for calculating thermal comfort index is a more convenient and fast way than the actual measurement, and its reliability has been verified by many researchers. Cinzia Buratti et al. (Cinzia Buratti, 2017) used simulated temperature parameters in the classroom of the University of Perugia to calculate the predicted thermal sensation. Paige Wenbin Tien and John Kaiser Calautit (Paige Wenbin Tien, 2019) used computational fluid dynamics CFD model to study the thermal comfort of high-rise buildings with different air courtyards. The results show that the design of air courtyards has little effect on the thermal comfort of buildings without considering vegetation. It is also suitable for local thermal comfort. Sally Shahzad et al. (Sally Shahzad, 2017) analyzed the performance of the chair by CFD simulation, and analyzed the thermal distribution around the hot chair with cushion in detail. The results show that improving the local thermal sensation of human body can improve the overall thermal comfort of human body. In this paper, a three-dimensional steady-state computational fluid dynamics (CFD) model is established by using the renormalization group (RNG) k- $\epsilon$  turbulence model to predict the air flow and temperature distribution. Combined with the adaptive thermal comfort model, the thermal comfort of each location in the natural ventilated residential space is evaluated, and the effects of solar radiation and ventilation on thermal comfort are studied. Firstly, the FLUENT software is used to simulate the indoor flow field and temperature field under different weather conditions, and the CFD model is validated by the measured data. The process of measurement and modeling will be described in detail in Chapter 2. Then, the influence of solar radiation and ventilation on thermal comfort is analyzed by comparing the simulation results with the indoor thermal comfort temperature predicted by the adaptive thermal comfort model. The part is discussed in Chapter 3.

## **2 METHOD**

### **2.1 Measurement**

This paper studies the thermal comfort of naturally ventilated residential buildings under different solar radiation. A residential building in Changsha was selected as the research object. The residence is one of the apartment buildings, and the horizontal distribution of the residence is shown in Figure 1. The out-of-plane normal of window one points to 45 degrees north-west. As shown in Table 1, the sizes of the interior doors are the same, and the sizes and forms of the three windows are different.

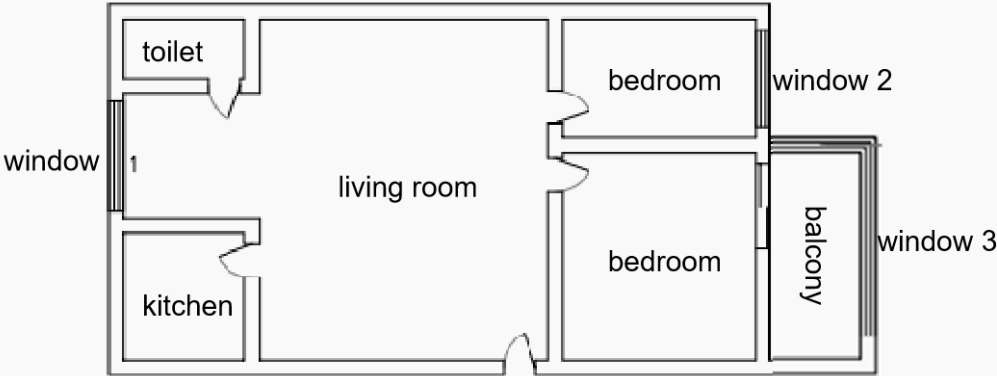

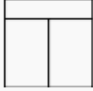

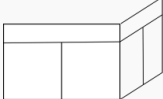


Figure 1: Residential plane

In order to obtain the actual indoor environmental parameters, HOBO was used to test and record the hourly temperature and humidity values from March 23 to May 13, 2019. HOBO is set to update and record data every 30 minutes. It is placed in the living room, bedroom and balcony room for testing. The test data will be used to validate the CFD model and thermal comfort analysis.

Table 1: Size and style of doors and windows

name	size	style
door	800mm*2000mm	
Window1	1460mm*1460mm	
Window2	1300mm*1650mm	
Window3	2800mm*1650mm+1400mm*1650mm	

## 2.2 CFD simulation

Figure 2 is a physical model built by CFD ICEM according to the above residential dimensions. To study the CFD model of natural ventilation, it is necessary to determine the external computational domain. The selection of computational domain is three times as much

as that of the building according to the general requirements (Atish Dixit, 2015). The grid division is shown in Figure 3. The height of computational domain is 8400 mm, the width is 19200 mm, the length is 40440 mm, and the distance between inlet and residence is 10110 mm. After trial calculation, the computational domain is sufficient for the full development of turbulence in the rear of the building, and the far-end air flow does not affect the indoor ventilation. Because the physical model is more standard, the structured grid is chosen. The size of the grid is related to the accuracy of computation and the amount of computing resources used. Different sizes are selected for grid division in different regions, and the grid in external computing domain is larger. The main object of study is the building part, which is refined. For the areas with complex flow and high wind speed, such as windows and doorframes, the grid is further refined. In order to avoid the influence of the number of meshes on the calculation results, grid independence verification was carried out. The initial number of meshes was 41594, the mesh quality was 0.98, the maximum draw ratio was 1.8, and the ventilation volume was calculated to be 1.263 kg/s. As shown in Table 2, when the number of grids exceeds 1 million, the calculation results are hardly affected by the number of grids, so the final grid is 1146 752.

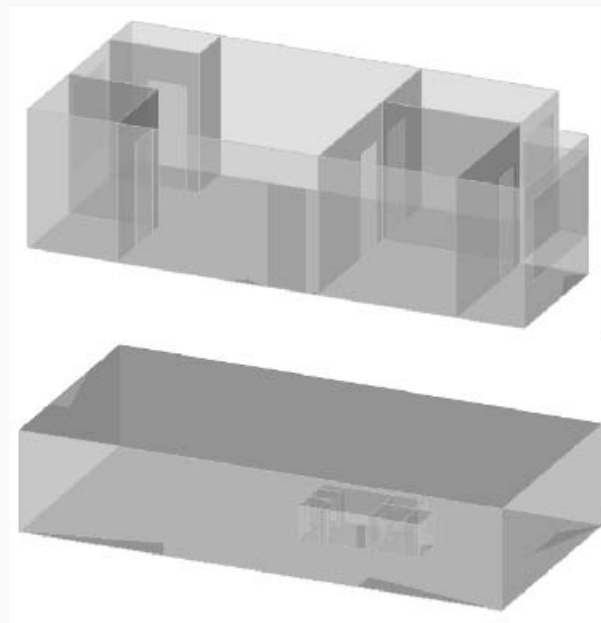


Figure 2: Physical model

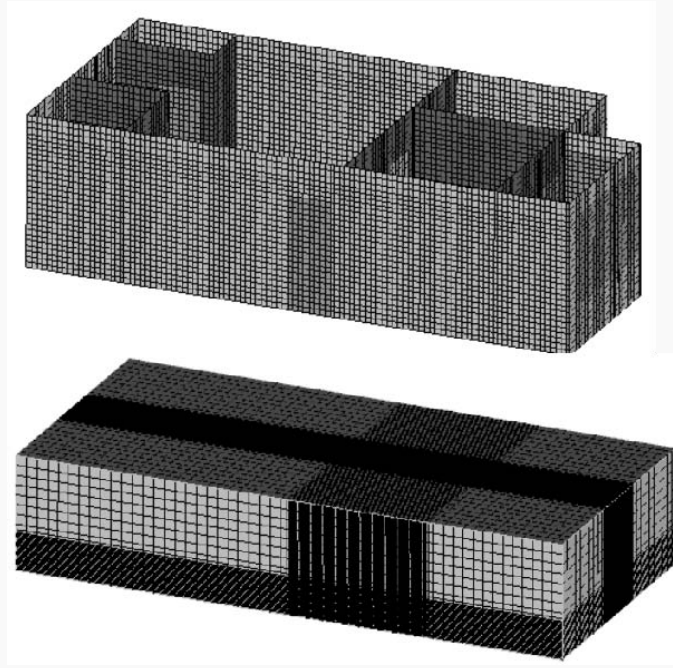


Figure 3: Mesh generation

Outdoor wind speed and direction change with time. Hourly wind speed monitored by meteorology can intuitively reflect outdoor weather change of natural ventilation, but the calculation cost is very large. The wind direction of natural ventilation is always changing, and the actual flow is transient. This brings difficulties to the determination of the entrance boundary conditions. Aiming at the exploratory study of the effects of simulation and solar radiation on thermal comfort in this paper, the representative outdoor wind speed is selected to simulate in steady state, which can achieve the purpose of this study. The front of the building is 45 degrees south to west. For the convenience of research, this paper chooses the direction of inflow parallel to the normal line of the front of the building, so the actual flow is simplified to steady flow with steady wind direction.

Table 2: Grid independence verification

	Test 1	Test 2	Test 3	Test 4
Number	415954	724389	1146752	1318247
Mass flow rate (kg/s)	1.263	1.524	1.654	1.683

Inlet boundary condition chooses the velocity entrance boundary condition, and the average velocity setting value takes the outdoor parameters of the hour. Turbulence intensity  $I$  and turbulence length size  $L$  are determined by formula(1) and (2).

$$(1) \quad I = 0.16Re^{-1/8}$$

$$(2) \quad L = 0.07D$$

Re is Reynolds number and D is pipe size. The pressure boundary condition is used for the outlet boundary condition. Pressure boundary conditions are used when flow details are not clear, but boundary pressures are known. When the outflow area is far from the backflow area and the flow direction does not change, the pressure boundary condition can be used. The outlet of the calculation area is natural outflow, and the outlet pressure is set as environmental pressure.

There is no indoor design temperature in the natural ventilation room, and the heat flow of the external wall can not be calculated as that of the air-conditioned room. Therefore, the known surface temperature of the external wall is used as the first kind of thermal boundary condition in CFD simulation. The outer wall is simplified as isotropic material, and the heat transfer from the outer surface to the inner surface is one-dimensional heat conduction. The thermal boundary condition is treated by steady state. The building maintenance structure is divided into inner wall and outer wall. The inner wall is considered as adiabatic boundary. The outer wall takes into account the influence of solar radiation and adopts outdoor comprehensive temperature. The outer walls and roofs in Southeast and southwest China are heated by solar radiation and outdoor air temperature. Considering the temperature rise caused by solar radiation, e.g. Formula 3, the outdoor comprehensive temperature is used to calculate the surface temperature of maintenance structures.

$$t_z = t_w + \frac{\alpha_s I}{\alpha_w} \quad (3)$$

Where,  $t_z$  is the outdoor comprehensive temperature;  $t_w$  is the calculated temperature of outdoor air;  $\alpha_s$  is the absorption coefficient of solar radiation on the outer surface of the maintenance structure;  $I$  is the total solar radiation illumination outside the maintenance structure;  $\alpha_w$  is the heat transfer coefficient of the outer surface of the maintenance structure. Symmetrical boundary conditions are used for calculating domain boundaries; doors in the room are assumed to be open and set to interior; windows are set to wall according to the opening and closing state of windows, and solar ray tracing is performed if they are closed; and windows are set to interface to connect indoor and outdoor air.

The CFD simulation in this paper is based on pressure-based solution, and SIMPLE algorithm is used. The pressure and momentum are solved by two-stage upwind method. Using the renormalization group (RNG) k-e turbulence model, K and E are solved by the first-order upwind scheme.

### 2.3 Model Verification

Temperature changes over time were recorded at three sites on April 17. The positions of three measuring points in the model were A (1.82, 3.9, 1.35), B (7.21, 4.4, 1.35), C (8.71, 9.75, 1.35). Point A is in the living room, Point B is in the bedroom and Point C is on the balcony. The simulated instantaneous temperature is compared with the measured temperature, as shown in Figure 4. In the picture, the test temperature (light red line) and the simulated temperature (dark red line) at the bedroom measuring point B basically coincide with each other, and the deviation is the smallest. The average temperature difference between 0 and 23 points is 0.6, 0.3 and 0.45, respectively.

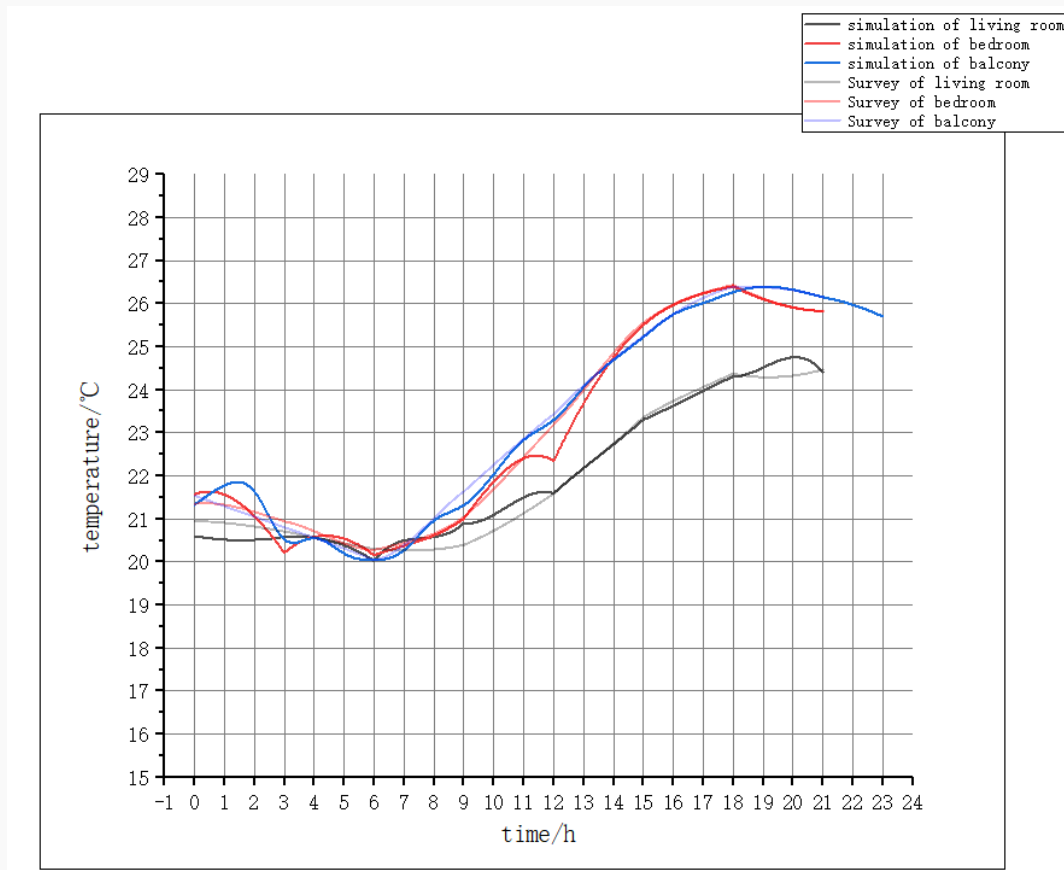


Figure 4: Comparison of test temperature with simulated temperature

## 2.4 Indoor Temperature Distribution

Figure 5 shows the temperature distribution in seven different rooms. Temperature fields at 8:00, 10:00, 12:00 and 2:00, 4:00 and 6:00 p.m. were simulated in different daytime considering the size of solar radiation and the direction of direct solar radiation. No solar radiation at night was considered as a typical case. Residential windows are located in the Northwest direction, and the walls of the gates are connected with other households. Therefore, the wall temperature in the southwest is maintained at 17 - 22 C, and there is no big fluctuation. The highest local temperature in a day is around 10:00 a.m., because the balcony is located in the Southeast direction, and the window openings are large, the direct sunlight makes the temperature of the southeast wall and balcony room rise sharply. During the day, the highest average air in the room is 12 o'clock. At this time, not only the solar radiation is stronger, but also the heat of the outer wall is released into the room after a morning's heating, which makes the indoor temperature rise. Temperature distribution is the most uniform point is 0, at this time the wall temperature difference is not big, so the temperature of each room will not be very different. The overall temperature in the room rises first and then decreases with time, which is consistent with the trend of outdoor temperature, mainly affected by solar radiation.

Fig. 6, the indoor velocity distribution is obtained under the conditions of maximum ( $v=4.3\text{m/s}$ ) and minimum ( $v=0.9\text{m/s}$ ) outdoor hourly wind speed in a day. When the wind speed is relatively high, the air flow enters from the balcony window and flows through the living room of the

bedroom and exhausts from the window. The indoor air flow velocity is very small, but the direction is basically the same, and there is no obvious eddy current. When the wind speed is small, the indoor air flow rate changes dramatically, forming many eddies which make the air flow in the living room and bedroom not smooth. In fact, 8 a.m. and 6 p.m. are the two time points with the highest wind speed. The horizontal zoning of the living room temperature occurs because the air flow makes the temperature in the central area drop faster than that near the wall.

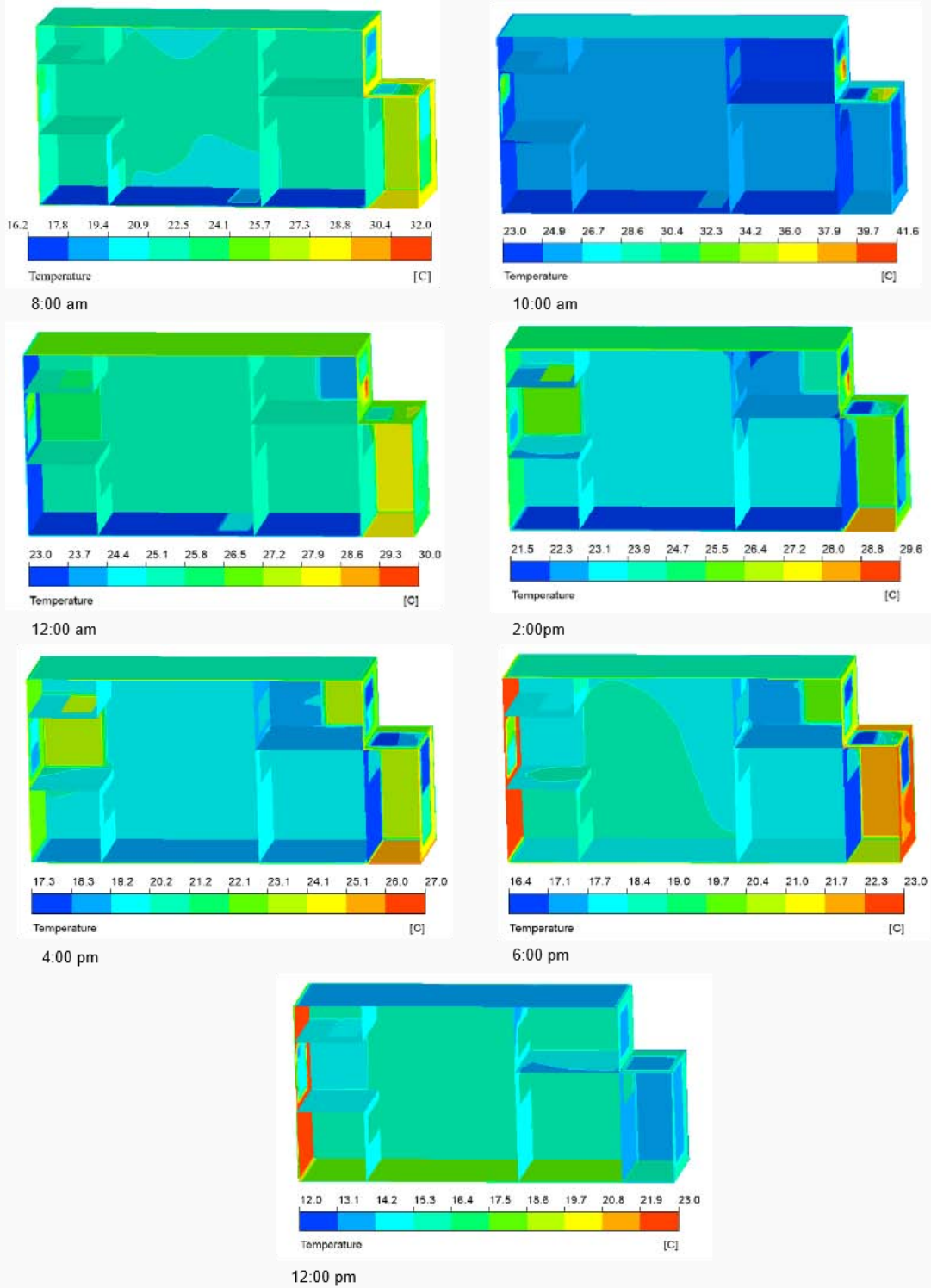


Figure 5: The Change of Temperature Field with Time



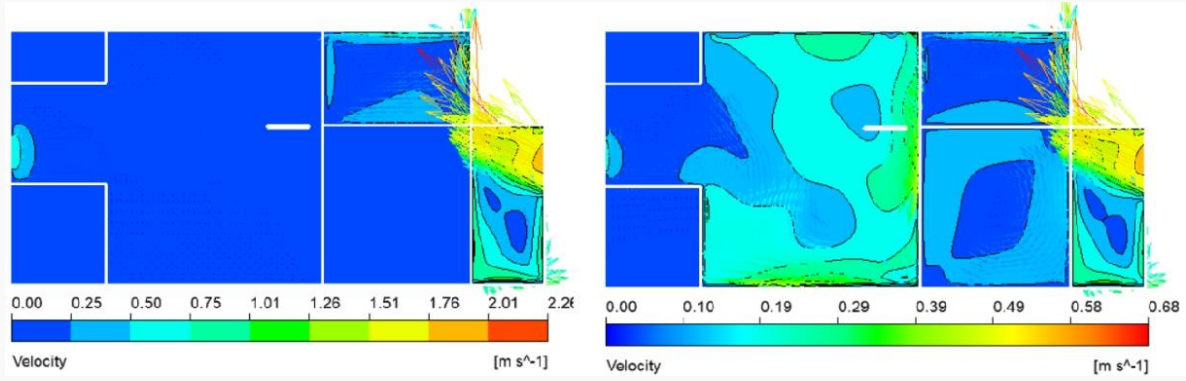


figure 6: Plane sketch of velocity field

## 2.5 Adaptive Thermal Comfort Index

The general method of evaluating with adaptive thermal comfort model is to calculate an average outdoor calculation parameter by using outdoor temperature of meteorological statistics. This parameter is called general average outdoor temperature or operating average outdoor temperature, e.g. formula (4). The recommended value  $\alpha=0.8$  and  $t_{e(d-n)}$  is the values of, the outdoor daily average temperatures from the date of calculation (ASHRAE, 2017).

$$t_{pma(out)} = (1-\alpha) \cdot [t_{e(d-1)} + \alpha \cdot t_{e(d-2)} + \alpha^2 \cdot t_{e(d-3)} + \alpha^4 \cdot t_{e(d-4)} + \dots] \quad (4)$$

The relationship between general average outdoor parameters or operating average outdoor temperature and upper and lower limits of indoor comfort temperature is a one-time function, that is, indoor comfort temperature conditions are determined by outdoor temperature. Figure 7 shows the relationship between indoor comfort temperature and general average outdoor temperature. The linear expression is shown in formula (5) and (6).

$$\begin{aligned} t_{up} &= 0.31t_{pma} + 21.3 \\ t_{lower} &= 0.31t_{pma} + 14.3 \end{aligned} \quad (5)$$

$$\begin{aligned} t_{up} &= 0.31t_{pma} + 20.3 \\ t_{lower} &= 0.31t_{pma} + 15.3 \end{aligned} \quad (6)$$

Formula(5) expresses the limit of 80% acceptance rate; and Formula(6) expresses the limit of 90% acceptance rate.

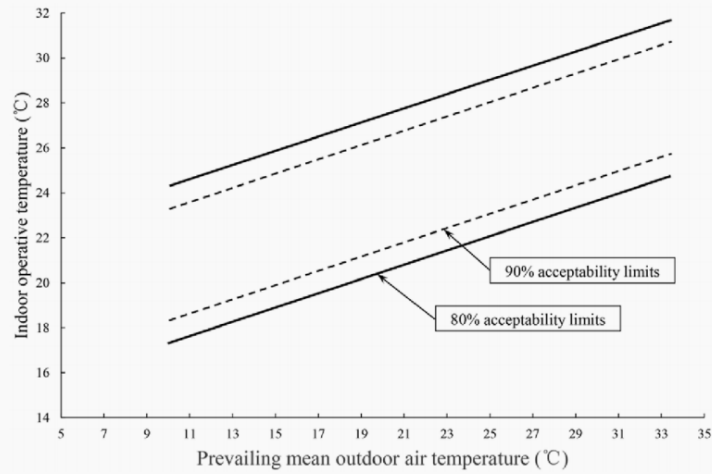


figure 7: Adaptive Thermal Comfort Model

From the above mathematical model, the range of comfortable temperature in the environment studied in this paper can be obtained. Figure 8 depicts the variation of acceptable comfort temperature in a day and the upper and lower limits of indoor temperature at different times. Obviously, we can judge the comfort by observing whether the indoor temperature is in the comfort zone. In the picture, the indoor temperatures from 21:00 to 23:00 and from 0:00 to 6:00 are all lower than the comfortable temperatures. However, because people should be sleeping during this period and have blankets and other insulation measures, they can not simply use the comfortable temperatures to judge, so this period of time will not be discussed. From 7:00 a.m. to 13:00 p.m. it's entirely within the comfort zone. From 14 p.m. to 20 p.m., part of the space is comfortable while the other part is uncomfortable. Next, we will distinguish the comfort zone from the uncomfortable zone in the room by analyzing the temperature field, and discuss what causes this.

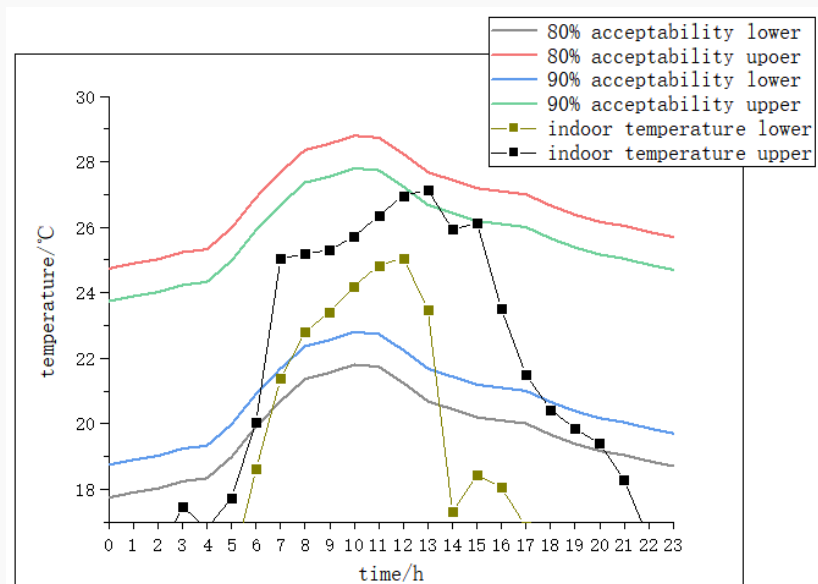


figure 8: Comparisons between Comfort Temperature and Simulated Temperature

Taking 15:00 as an example, Fig. 9 is a horizontal screenshot of temperature distribution at altitudes of 0.15m, 0.5m, 1.2m, 1.5m, 1.8m and 2.0m, respectively. These heights indicate the temperature of the ankle, knee, chest, head and upper region of the standing person,

respectively. The maximum vertical temperature difference is more than 7 °C, because the house is located on the top floor and heat is transmitted into the room through the roof.

According to the relevant vertebrae, when standing, the temperature difference between head and foot should satisfy  $\Delta t \leq 3^\circ\text{C}$ . However, only the balcony and the corner of the bedroom in the Northeast have more than comfortable temperature difference, which can be ignored, that is to say, in this case, the temperature difference between the upper and lower parts will not cause uncomfortable feeling. However, only the balcony and the corner of the bedroom in the Northeast have more than comfortable temperature difference, which can be ignored, that is to say, in this case, the temperature difference between the upper and lower parts will not cause uncomfortable feeling. According to the thermal comfort model, the comfort temperature at this time is 20.19 - 27.19 °C, and the temperature field at six altitudes is plotted within this temperature range. The area below the lower temperature limit is dark blue, and the area beyond the upper temperature limit is red. When  $Z < 0.5\text{m}$ , all areas of the room are below the comfortable temperature, reflecting a partial cold state. With the increase of height, the area with moderate temperature gradually enlarges, and the temperature gradually decreases from three outer walls to the inside. The room with transparent envelope structure, due to the role of solar radiation, the temperature change is faster and the difference is larger, the difference of local thermal comfort is more obvious; in contrast, the temperature distribution in the living room will be more uniform.

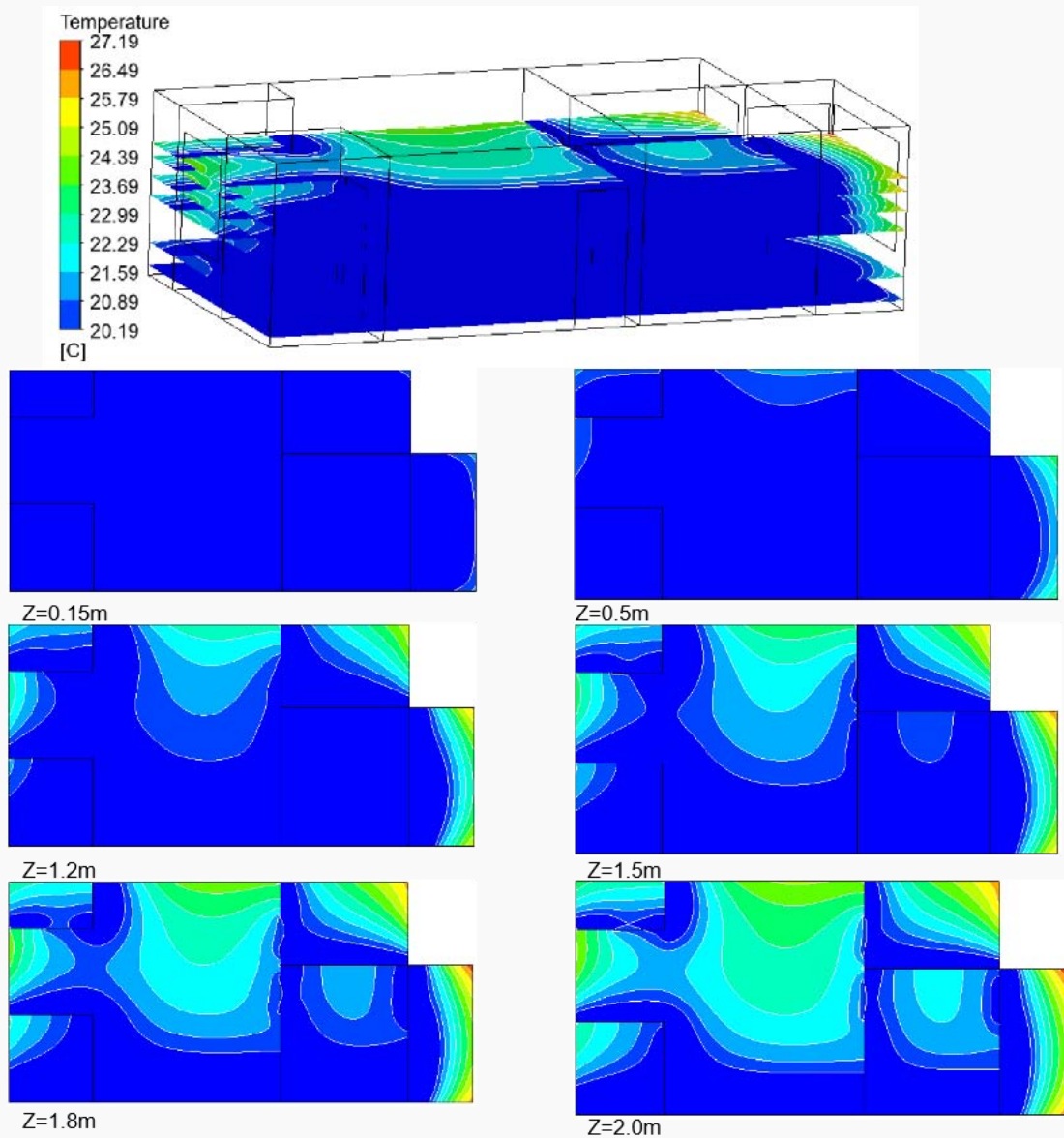


figure 9:Temperature Distribution at Different Heights

At the same time, that is, under the same conditions of solar radiation, the values of different thermal comfort indexes of ventilation volume are compared. Figure 10 depicts the relationship between thermal comfort and ventilation. There is no obvious consistency or relative relationship between the peak value and trend of curve describing comfort index and ventilation rate. Therefore, under the same solar radiation, the effect of ventilation rate on thermal comfort is not obvious, or there is no obvious linear relationship between them.

Figure 11 depicts the relationship between thermal comfort index and solar radiation. The value of solar radiation is determined by geographical location and time. According to the comparison of indoor temperature and comfortable temperature, thermal comfort index is evaluated with 1 as the most comfortable and 0 as the most uncomfortable. The changes of seven groups of data from 7:00 to 21:00 are counted and the trends of the two are observed. At first, the solar radiation gradually rises, and the thermal comfort index does not fluctuate significantly. They are basically in the most comfortable state. As the solar radiation begins to decrease, the thermal comfort is getting worse and worse. Until the solar radiation equals zero, the thermal comfort index is still getting lower and lower until it also drops to zero. It shows that the higher the solar

environment, and calculates the temperature and velocity distribution in the environment. Taking a unit house in Changsha as the research object, field tests were carried out to determine the parameters needed for thermal comfort and set input data. External air temperature, combined temperature and wind speed are used as input data in CFD program. The model was validated by checking the instantaneous temperatures at three different locations and applied to the prediction of indoor global and local thermal comfort. The thermal comfort evaluation method adopted in this paper is an adaptive thermal comfort model, and the thermal comfort index is obtained through the average parameters of outdoor temperature. The results show that during the transitional season, the whole indoor area is comfortable for about 6 hours a day, and only the part of the room whose exterior wall can be exposed to sunlight is comfortable for 6 to 8 hours. The temperature difference in the room is affected by the solar radiation, and increases with the increase of radiation. The maximum temperature difference is more than 8°C. The influence of solar radiation and ventilation rate on adaptive thermal comfort index is analyzed through data statistics. The results show that solar radiation has obvious influence on thermal comfort. In the case of this study, the higher the solar radiation is, the better the thermal comfort, but the difference of local thermal comfort will be greater; and the influence of ventilation rate on thermal comfort is not obvious.

#### 4 REFERENCES

- Richard de Dear (2001). *The adaptive model of thermal comfort and energy conservation in the built environment*. Int J Biometeorol (2001) 45:100 – 108
- C. Bouden, N. Ghrab.(2005). *An adaptive thermal comfort model for the Tunisian context*. Energy and Buildings 37 : 952–963.
- J.I. Peren (2015). *CFD analysis of cross-ventilation of a generic isolated building with asymmetric opening positions: Impact of roof angle and opening location*. Building and Environment 85: 263-276
- H.Montazeri, F. Montazeri.(2018). *CFD simulation of cross-ventilation in buildings using rooftop windcatchers: Impact of outlet openings*. Renewable Energy 118: 502-520.
- Xiufeng Yang.(2015). *Numerical investigation on the airflow characteristics and thermal comfort in buoyancy-driven natural ventilation rooms*. Energy and Buildings 109 : 255 – 266.

Cinzia Buratti et al. (2017). *Prediction Of Indoor Conditions And Thermal Comfort Using CFD Simulations: A Case Study Based On Experimental Data*. Energy Procedia 126 :115 - 122

Paige Wenbin Tien (2019). *Numerical analysis of the wind and thermal comfort in courtyards “skycourts” in high rise buildings*. Journal of Building Engineering 24 : 100735

Sally Shahzad et al. (2017). *A user-controlled thermal chair for an open plan workplace: CFD and field studies of thermal comfort performance*. Applied Energy 207 : 283 - 293

Atish Dixit (2015). *A case study on human bio-heat transfer and thermal comfort within CFD*. Building and Environment 94:122-130

American Society of Heating, Refrigerating and Air- Conditioning Engineers (2017). *ANSI/ASHRAE, ANSI/ASHRAE Standard 55-Thermal Environmental Conditions for Human Occupancy*.